Chinese Journal of Natural Medicines

Eudesmane–guaiane sesquiterpenoid dimers from *Aucklandia costus* trigger paraptosis–like cell death *via* ROS accumulation and MAPK hyperactivation

Longgao XIAO, Yueqin ZHAO, Xiao DING, Hui LIU, Guangyu ZHU, Yanxi LI, Huan YAN, Xin FANG, Yuhan ZHAO, Haiyang LIU

Citation: Longgao XIAO, Yueqin ZHAO, Xiao DING, Hui LIU, Guangyu ZHU, Yanxi LI, Huan YAN, Xin FANG, Yuhan ZHAO, Haiyang LIU, Eudesmane–guaiane sesquiterpenoid dimers from *Aucklandia costus* trigger paraptosis–like cell death *via* ROS accumulation and MAPK hyperactivation, Chinese Journal of Natural Medicines, 2024, 22(11), 1–10. doi: 10.1016/S1875–5364(24)60592–3.

View online: https://doi.org/10.1016/S1875–5364(24)60592–3

Available online at www.sciencedirect.com
ScienceDirect
Chinese Journal of Natural Medicines 2024, **22**(11): 1011-1019
doi: 10.1016/S1875-5364(24)60592-3
Chinese Journal of Natural Medicines

•Original article•

Eudesmane-guaiane sesquiterpenoid dimers from *Aucklandia costus* trigger paraptosis-like cell death *via* ROS accumulation and MAPK hyperactivation

XIAO Longgao[1, 2Δ], ZHAO Yueqin[1, 2Δ], DING Xiao[1], LIU Hui[1], ZHU Guangyu[1, 2], LI Yanxi[1], YAN Huan[1], FANG Xin[1*], ZHAO Yuhan[1*], LIU Haiyang[1, 3*]

[1] *State Key Laboratory of Phytochemistry and Plant Resources in West China, and Yunnan Key Laboratory of Natural Medicinal Chemistry, Kunming Institute of Botany, Chinese Academy of Sciences, Kunming 650201, China;*
[2] *University of Chinese Academy of Sciences, Beijing 100049, China;*
[3] *Yunnan Characteristic Plant Extraction Laboratory, Kunming 650106, China*

Available online 20 Nov., 2024

[ABSTRACT] Three novel sesquiterpenoid heterodimers, designated as auckcostusolides A–C (**1**–**3**), were isolated from *Aucklandia costus* leaves. The structures of compounds **1**–**3** were elucidated through comprehensive spectroscopic analysis, with their absolute configurations established using a combination of X-ray single-crystal diffraction and electronic circular dichroism (ECD) calculations. Notably, compounds **1** and **2**, despite sharing identical planar structures derived from two identical sesquiterpenoids, exhibited opposite configurations at C-11 and C-8′. This configurational difference can be attributed to distinct Diels−Alder cycloaddition processes between the sesquiterpenoid monomers. Additionally, the cytotoxic effects of compounds **1**–**3** were evaluated against colorectal cancer HCT116 cells, fibrosarcoma HT1080 cells, and hepatocellular carcinoma HepG2 cells. Compounds **1**–**3** induced cell death was characterized by endoplasmic reticulum (ER) swelling and cytoplasmic vacuolization, typical morphological changes associated with paraptosis. Mechanistic studies revealed that compounds **1** and **3** triggered paraptosis-like cell death through the accumulation of reactive oxygen species (ROS), activation of ER stress, and stimulation of the MAPK signaling pathway.

[KEY WORDS] *Aucklandia costus*; Sesquiterpenoid heterodimers; Auckcostusolides A–C; Paraptosis; MAPK signaling pathway
[CLC Number] R965, R917 **[Document code]** A **[Article ID]** 2095-6975(2024)11-1011-09

Introduction

Paraptosis, initially described in 2000, is a form of programmed cell death (PCD) characterized by cytoplasmic vacuolation, typically involving endoplasmic reticulum (ER) or mitochondrial swelling [1]. Research has shown that paraptosis, beyond its role in cancer, is implicated in various processes, including development, neurodegeneration, responses to viral and bacterial infections, and conditions such as glaucoma [2]. The discovery of paraptosis modulators presents a promising potential treatment approach for these diseases, including cancers. In recent years, several natural products have been reported to induce paraptosis and inhibit cancer cell proliferation [2–5]. Consequently, paraptosis inducers represent an attractive alternative strategy for cancer therapy, particularly for cases resistant to other forms of PCD.

Aucklandia costus Falc., also known as *Saussurea costus*, is a perennial tall herbaceous plant belonging to the genus *Aucklandia* (Asteraceae family). Originally introduced from India, *A. costus* has been extensively cultivated in Southwest China [6]. As a valuable medicinal plant, *A. costus* is widely utilized for treating stomach problems, ulcers, asthma, and inflammatory diseases [7]. Beyond its medi-

[Received on] 18-Feb.-2024
[Research funding] This work was supported by Yunnan Revitalization Talent Support Program "Top Team" Project (No. 202305AT350001), "Young Talent" Project (No. YNQR-QNRC-2019-091), the National Natural Science Foundation of China (Nos. 32170408, 32000280, and 32000548), the Ten Thousand Talents Plan of Yunnan Province for Industrial Technology Leading Talents (No. YNWR-CYJS-2019-011), the Project of Yunnan Characteristic Plant Screening and R&D Service CXO Platform (No. 2022YKZY001), the CAS Pioneer Hundred Talents Program, the Training of Technological Innovation Talents of Yunnan Province (No. 202305AD160009), the Special Research Assistant of Chinese Academy of Sciences (No. E3292211Q1), and the Young Academic and Technical Leader Raising Foundation of Yunnan Province (No. 202005AC160035).
[*]**Corresponding author]** E-mails: xinfang@mail.kib.ac.cn (FANG Xin); zhaoyuhan@mail.kib.ac.cn (ZHAO Yuhan); haiyangliu@mail.kib.ac.cn (LIU Haiyang)
[Δ]These authors contributed equally to this work.
These authors have no conflict of interest to declare.

cinal applications, the roots of *A. costus* have been approved as a functional food by the National Health Commission of the People's Republic of China. Moreover, the seeds of *A. costus* are edible, and the dried leaves are used for tobacco, firewood, and feeding purposes [7–10]. The process of elucidating the pharmacodynamic basis of *A. costus* roots has led to the discovery of several bioactive terpenoids, particularly sesquiterpenoids containing an *α*-methylene-*γ*-butyrolactone moiety [11, 12]. Among these, costunolide and dehydrocostus lactone have been extensively studied for their ability to induce cell cycle arrest and apoptosis in various tumor cells [13]. Additionally, a small quantity of sesquiterpenoid dimers were isolated from the roots of *A. costus*, primarily formed through Diels−Alder cycloaddition with two distinct types of sesquiterpenoids. Pharmacological studies indicated that these dimers exhibited cytotoxicity and anti-inflammatory activities [14–17]. While a limited number of studies have indicated the potential anti-tumor activity of the crude extract of *A. costus* leaves, there is a notable lack of research regarding the phytochemicals of *A. costus* leaves [18]. During our investigation of alternative medicinal molecules from *A. costus*, three new eudesmane-guaiane sesquiterpenoid dimers, named auckcostusolides A–C (**1**–**3**) (Fig. 1), were isolated from its leaves. Furthermore, compounds **1**–**3** were evaluated for their cytotoxicity against three tumor cell lines, and were found to trigger paraptosis-like cell death. Mechanistically, compounds **1** and **3** induced paraptosis-like cell death by increasing the accumulation of reactive oxygen species (ROS). Moreover, the paraptosis-like cell death was mediated by the induction of ER stress and the hyperactivation of the MAPK signaling pathway. Herein, we report the isolation, structural elucidation, and potential anti-tumor activities of **1**–**3**.

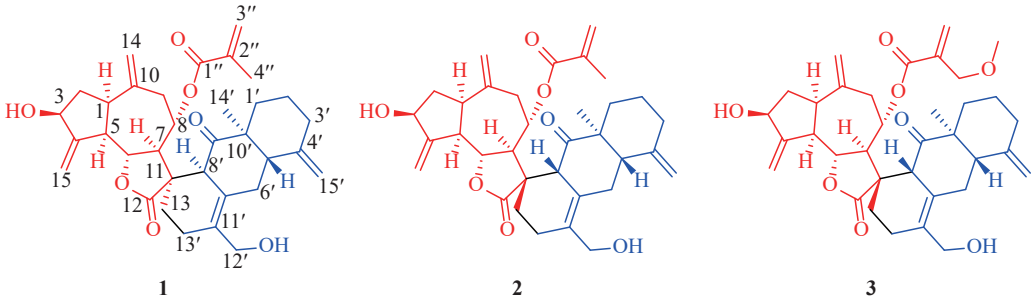

Fig. 1 Structures of compounds 1–3.

Results and Discussion

Auckcostusolide A (**1**), colorless needle crystals (*n*-hexane/acetone, 4 : 1, *V/V*), exhibited a molecular formula of $C_{34}H_{42}O_7$ with fourteen degrees of unsaturation (DOUs), as determined by HR-ESI-MS spectrum (ion peak at *m/z* 585.2827 $[M + Na]^+$, Calcd. for $C_{34}H_{42}NaO_7^+$, 585.2828, Fig. S9). The IR spectrum revealed characteristic absorption bands indicating the presence of hydroxyl (3433 cm^{-1}), carbonyl (1752 and 1713 cm^{-1}), and olefinic (1640 cm^{-1}) functionalities. The ^1H NMR spectral data (Table 1) displayed signals of two methyl groups at δ_H 1.08 (s, 3H) and 1.94 (s, 3H), one oxygenated methylene at δ_H 4.11 (d, J = 11.8 Hz, 1H) and 4.21 (d, J = 11.8 Hz, 1H), three oxygenated methines [δ_H 4.52 (m, 1H), 4.56 (dd, J = 10.7, 9.2 Hz, 1H), and δ_H 4.64 (m, 1H)], and four exocyclic methylene groups [δ_H 4.65 (s, 1H) and 4.91 (s, 1H), 4.75 (s, 1H) and 5.08 (s, 1H), 5.38 (s, 1H) and 5.57 (s, 1H), 5.63 (s, 1H) and 6.12 (s, 1H)]. The ^{13}C NMR and DEPT spectroscopic data (Table 1) revealed the presence of 34 carbon resonances, including three carbonyls (δ_C 166.5, 178.1, and 214.4), ten olefinic carbons (δ_C 108.4, 114.2, 117.6, 126.9, 128.9, 130.9, 136.1, 142.3, 147.4, and 152.8), nine sp^3 methylenes including one oxygenated (δ_C 62.9), eight sp^3 methines with three oxygenated (δ_C 71.1, 74.0, and 78.5), two methyls, and two sp^3 quaternary carbons. Additionally, a set of NMR signals [δ_H 1.94 (s, 3H), 5.63 (s, 1H) and 6.12 (s, 1H); δ_C 18.5, 126.9, 136.1, and 166.5] indicated the presence of a 2-methylacryloyl moiety [19]. In the absence of a benzene ring, the remaining 30 carbon resonances and twelve DOUs suggested that compound **1** might be a sesquiterpenoid dimer.

The planar structure of compound **1** was elucidated through comprehensive analysis of ^1H–^1H correlation spectroscopy (COSY) and heteronuclear multiple bond correlations (HMBCs) (Fig. 2). The ^1H–^1H COSY correlations of H-3/H_2-2/H-1/H-5/H-6/H-7/H-8/H_2-9, in conjunction with HMBCs from H_2-15 to C-3, C-4, and C-5, from H_2-14 to C-1, C-9, and C-10, and from H-7 to C-11 and C-13 established the guaianolide core. The lactone ring formation was inferred from the chemical shifts of C-6 (δ_C 78.5, indicating an oxygenated methine) and C-12 (δ_C 178.1, indicating an ester carbonyl), alongside the HMBC from H-6 to C-12. The 2-methylacryloyl moiety, attached to the guaianolide core at C-8, was confirmed by HMBCs from H_2-3″ to C-1″, C-2″, and C-4″, from H_3-4″ to C-1″, and from H-8 to C-1″. Moreover, the presence of 3-OH was substantiated by the chemical shift of C-3 (δ_C 74.0, indicating an oxygenated methine) and the absence of HMBCs from H-3 to an ester carbonyl or oxygenated sp^3 carbons. Additionally, the ^1H–^1H COSY correlations of H_2-1′/H_2-2′/H_2-3′ and H-5′/H_2-6′, combined with HMBCs from H_2-15′ to C-3′, C-4′, and C-5′, from H_3-14′ to C-1′, C-5′, C-9′, and C-10′, from H_2-12′ to C-7′, C-11′, and C-13′, H-8′ to C-9′ and C-11′, and from H-6′ to C-7′ established the eudesmane unit. The NMR signals [δ_H 4.11 (d, J = 11.8 Hz, 1H) and 4.21 (d, J = 11.8 Hz, 1H); δ_C 62.9] indicated the

Table 1 ^{1}H (500 MHz) and ^{13}C (125 MHz) NMR spectroscopic data of compounds **1**–**3** in $CDCl_3$.

No.	1		2		No.	3	
	δ_H (mult., *J* in Hz)	δ_C, types	δ_H (mult., *J* in Hz)	δ_C, types		δ_H (mult., *J* in Hz)	δ_C, types
1	2.92, m	45.6, CH	2.94, q (8.9)	44.4, CH	1	2.95, q (8.8)	44.4, CH
2α	2.14, m	39.8, CH_2	2.27, m	38.9, CH_2	2α	2.28, dd (13.8, 7.1)	38.9, CH_2
2β	1.72, m		1.72, overlapped		2β	1.72, m	
3	4.52, m	74.0, CH	4.54, t (6.9)	74.0, CH	3	4.54, t (7.0)	74.0, CH
4		152.8, C		152.9, C	4		152.9, C
5	2.76, t (9.7)	52.9, CH	3.14, overlapped	50.5, CH	5	3.15, overlapped	50.5, CH
6	4.56, dd (10.7, 9.2)	78.5, CH	4.22, t (10.0)	77.5, CH	6	4.22, t (10.1)	77.5, CH
7	2.37, t (9.7)	55.1, CH	3.13, overlapped	52.4, CH	7	3.13, overlapped	52.3, CH
8	4.64, m	71.1, CH	5.07, ddd (10.9, 6.6, 4.6)	72.4, CH	8	5.11, m	72.6, CH
9α	2.30, dd (15.0, 2.2)	35.1, CH_2	2.20, dd (13.4, 6.7)	39.6, CH_2	9α	2.21, dd (13.4, 6.6)	39.7, CH_2
9β	2.49, dd (15.1, 4.7)		2.72, dd (13.4, 4.6)		9β	2.73, dd (13.4, 4.7)	
10		142.3, C		142.3, C	10		142.2, C
11		44.6, C		46.3, C	11		46.3, C
12		178.1, C		176.9, C	12		176.9, C
13a	1.89, m	36.0, CH_2	1.88, m	24.5, CH_2	13a	1.87, dd (13.1, 3.1)	24.5, CH_2
13b	1.83, m		1.58, m		13b	1.57, overlapped	
14a	5.08, s	117.6, CH_2	5.10, s	117.1, CH_2	14a	5.11, s	117.1, CH_2
14b	4.75, s		4.98, s		14b	4.98, s	
15a	5.57, s	114.2, CH_2	5.54, s	113.3, CH_2	15a	5.55, s	113.2, CH_2
15b	5.38, s		5.35, s		15b	5.35, s	
1′α	1.51, m	33.1, CH_2	2.01, d (13.1)	34.9, CH_2	1′α	2.01, d (13.3)	34.9, CH_2
1′β	1.81, m		1.38, td (13.3, 4.0)		1′β	1.40, td (13.3, 3.8)	
2′α	1.50, m	22.5, CH_2	1.56, m	22.6, CH_2	2′α	1.56, overlapped	22.6, CH_2
2′β	1.71, m		1.72, overlapped		2′β	1.73, overlapped	
3′α	2.28, m	36.4, CH_2	2.38, m	36.4, CH_2	3′α	2.37, d (13.2)	36.3, CH_2
3′β	1.88, m		1.92, m		3′β	1.94, td (13.3, 4.8)	
4′		147.4, C		147.1, C	4′		147.2, C
5′	2.11, m	47.0, CH	2.42, m	42.1, CH	5′	2.51, m	41.8, CH
6′α	2.18, m	27.0, CH_2	2.61, m	25.9, CH_2	6′α	2.59, d (15.3)	26.0, CH_2
6′β	2.91, m		2.50, m		6′β	2.51, m	
7′		128.9, C		123.3, C	7′		123.6, C
8′	3.49, br s	53.4, CH	3.72, overlapped	52.6, CH	8′	3.75, br s	52.6, CH
9′		214.4, C		213.9, C	9′		214.1, C
10′		50.0, C		48.6, C	10′		48.5, C
11′		130.9, C		132.5, C	11′		132.2, C
12'a	4.21, d (11.8)	62.9, CH_2	4.23, d (11.8)	62.5, CH_2	12'a	4.19, overlapped	62.5, CH_2
12'b	4.11, d (11.8)		4.14, d (12.4)		12'b	4.15, overlapped	
13′a	2.62, m	25.3, CH_2	2.29, m	23.2, CH_2	13′a	2.29, m	23.2, CH_2
13′b	2.12, m		2.21, m		13′b	2.22, m	
14′	1.08, s	17.0, CH_3	0.85, s	15.2, CH_3	14′	0.85, s	15.2, CH_3
15′a	4.91, s	108.4, CH_2	4.93, s	108.8, CH_2	15′a	4.93, s	108.7, CH_2
15′b	4.65, s		4.68, s		15′b	4.67, s	
1″		166.5, C		166.0, C	1″		164.7, C
2″		136.1, C		136.5, C	2″		137.4, C
3″a	6.12, s	126.9, CH_2	6.05, s	126.2, CH_2	3″a	6.24, s	126.9, CH_2
3″b	5.63, s		5.63, s		3″b	5.89, s	
4″	1.94, s	18.5, CH_3	1.95, s	18.5, CH_3	4″a	4.15, d (13.7)	70.8, CH_2
					4″b	4.07, d (13.7)	
					4″-OCH_3	3.34, s	58.5, CH_3

presence of a methylol. Furthermore, the HMBCs from H_2-12′ to C-7′, C-11′, and C-13′, and from H_2-13 to C-11′ confirmed the location of $\Delta^{7',11'}$. The connection of guaianolide and eudesmane units *via* two C–C bonds of C-11/C-8′ and C-13/C-13′ was verified by the ^{1}H–^{1}H COSY correlation of H_2-13/H_2-13′ and HMBCs from H-7 to C-8′, H-8′ to C-12, and H-13 to C-11′. Consequently, the planar structure of **1** was determined, as illustrated in Fig. 2.

The relative configuration of **1** was elucidated through rotating frame nuclear overhauser effect spectroscopy (ROESY) experiment analysis, as depicted in Fig. 2. Within the guaianolide unit, ROESY correlations of H-1/H-3/H-5/H-7, H-5/H-2α (δ_H 2.14) indicated their co-facial orientation, arbitrarily assigned as *α*-oriented. ROESY correlations of H-2β (δ_H 1.72)/H-9β (δ_H 2.49)/H-6 and H-9β/H-8 revealed their *β*-orientation. In the eudesmane unit, ROESY correlations of H_3-14′/H-8′/H-6′α (δ_H 2.18) indicated their co-facial orientation, assigned as *α*-oriented. The ROESY correlation of H-6′β (δ_H 2.91)/H-5′ revealed their *β*-orientation. The ROESY correlation between H-7 and H_2-13 suggested that H_2-13 and the

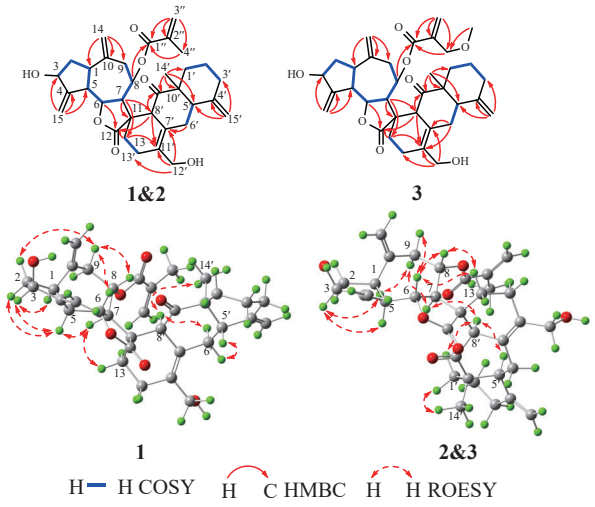

Fig. 2 The key 2D NMR correlations of compounds 1–3.

fused cyclohexene were *α*-oriented. To determine the absolute configuration of compound **1**, ECD calculations were performed at the b3lyp/6-311 + g(2d, p) level using the PCM model in methanol. The experimental CD curve closely matched the calculated ECD of (1*R*, 3*S*, 5*R*, 6*R*, 7*R*, 8*S*, 11*S*, 5′*S*, 8′*S*, 10′*S*)-**1** (**1a**) (Fig. 3). Furthermore, suitable crystals of 1 were obtained in *n*-hexane/acetone (4 : 1, *V/V*), enabling single-crystal X-ray diffraction (XRD) analysis using Cu K α radiation [flack parameter = 0.11(9)] (Fig. 4). The combination of ECD calculations and single-crystal XRD analysis unequivocally established the absolute configuration of compound **1** as 1*R*, 3*S*, 5*R*, 6*R*, 7*R*, 8*S*, 11*S*, 5′*S*, 8′*S*, 10′*S*.

Auckcostusolide B (**2**), obtained as a white amorphous powder, exhibited a molecular formula of $C_{34}H_{42}O_7$ with fourteen DOUs, as determined by HR-ESI-MS spectrum (ion peak at *m/z* 585.2827 $[M + Na]^+$, Calcd. for $C_{34}H_{42}NaO_7^+$, 585.2828, Fig. S19). The IR characteristic absorption bands indicated the presence of hydroxyl (3429 cm^{-1}), carbonyl (1768 and 1710 cm^{-1}), and olefinic (1638 cm^{-1}) functionalities. Comprehensive analyses of 1D and 2D NMR (Table 1 and Fig. 2) and MS data suggested that compound **2** possessed the same planar structure as compound **1**. However, notable differences in carbon chemical shifts between compounds **1** and **2**, particularly at C-13 and C-7′ were observed. This information indicated that compound **2** was a diastereoisomer of **1**. In the ROESY spectrum (Fig. 2), the cross peaks of H-5/H-3/H-1/H-9α (δ_H 2.20)/H-7 indicated their co-facial orientation and were assigned as *α*-oriented. The ROESY correlations of H-9β (δ_H 2.72)/H-6/H-8 revealed their *β*-orientation. In the eudesmane unit, the ROESY correlations of H_3-14′/H-1′α (δ_H 1.38) indicated their co-facial orientation, and were assigned as *α*-oriented. The ROESY correlations of H-1′β (δ_H 2.01)/H-8′/H-5′ revealed their *β*-orientation. The ROESY correlation of H-6/H_2-13/H-8 suggested that H_2-13 and the fused cyclohexene were in the *β*-direction. Furthermore, the absolute configuration of compound **2** was determined as 1*R*, 3*S*, 5*R*, 6*R*, 7*R*, 8*S*, 11*R*, 5′*S* , 8′*R*, 10′*S* through ECD calculations (Fig. 3).

Auckcostusolide C (**3**), a white amorphous powder, exhibited a molecular formula of $C_{35}H_{44}O_8$ with fourteen DOUs, as determined by HR-ESI-MS spectrum (ion peak at *m/z* 615.2933 $[M + Na]^+$, Calcd. for $C_{35}H_{44}NaO_8^+$, 615.2934, Fig. S29). The IR characteristic absorption bands indicated the presence of hydroxyl (3436 cm^{-1}), carbonyl (1766 and 1711 cm^{-1}), and olefinic (1643 cm^{-1}) functionalities. The ^{1}H NMR spectral data (Table 1) revealed signals of two methyl groups, including one oxygenated at δ_H 0.85 (s, 3H) and 3.34 (s, 3H), two oxygenated methylenes at δ_H 4.07 (d, J = 13.7 Hz, 1H) and 4.15 (d, J = 13.7 Hz, 1H), 4.15 (o, 1H) and 4.19 (o, 1H), three oxygenated methines [δ_H 4.22 (t, J = 10.1 Hz, 1H), 4.54 (t, J = 7.0 Hz, 1H), and 5.11 (m, 1H)], and four exocyclic methylene groups [δ_H 4.67 (s, 1H) and 4.93 (s, 1H), 4.98 (s, 1H) and 5.11 (s, 1H), 5.35 (s, 1H) and 5.55 (s, 1H), 5.89 (s, 1H) and 6.24 (s, 1H)]. The ^{13}C NMR and DEPT spectroscopic data (Table 1) indicated the presence of 35 carbon resonances, including three carbonyls (δ_C 164.7, 176.9, and 214.1), ten olefinic carbons (δ_C 108.7, 113.2, 117.1, 123.6, 126.9, 132.2, 137.4, 142.2, 147.2, and 152.9), ten sp^3 methylenes including two oxygenated (δ_C 62.5 and 70.8), eight sp^3 methines with three oxygenated (δ_C 72.6, 74.0, and 77.5), two methyls with one oxygenated (δ_C 58.5), and two sp^3 quaternary carbons. The NMR data of compound **3** demonstrated high similarity to those of **2**, except that C-4″ in compound **3** was modified to oxygenated methylene (δ_C 70.8) and substituted by methoxy. The HMBCs from 4″-OCH_3 (δ_H 3.34) and H-3″ to C-4″ confirmed this observation (Fig. 2). According to the ROESY spectrum, compounds **2** and **3** showed the same relative configuration (Fig. 2). Furthermore, the absolute configuration of compound **3** was determined to be identical to that of compound **2** through ECD calculations (Fig. 3).

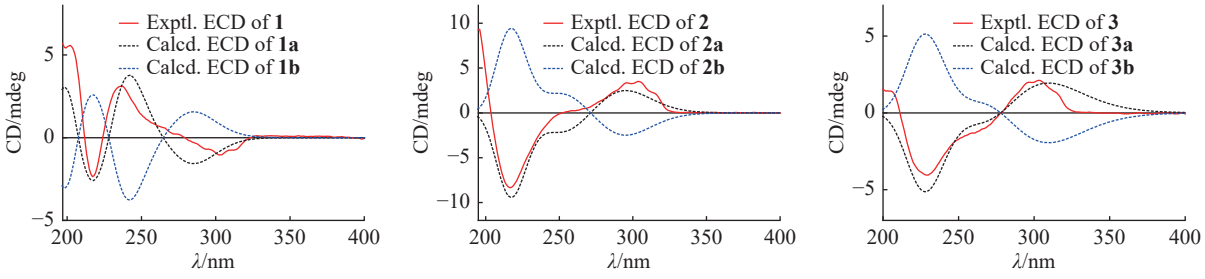

Fig. 3 Experimental and calculated ECD spectra for compounds 1–3 in MeOH.

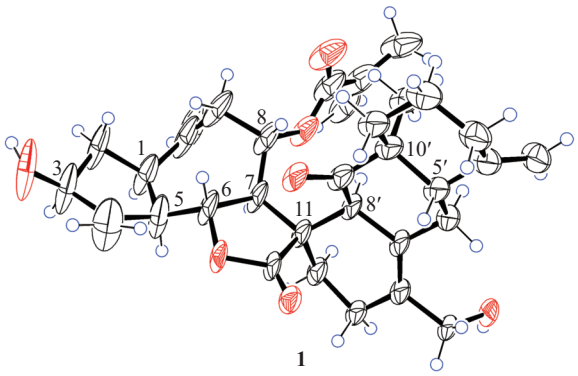

Fig. 4 Crystal structure of compound 1.

Biological activity

The cytotoxic effects of compounds **1**–**3** on different tumor cell lines (HCT116, HT1080, and HepG2) were evaluated using the MTT assay. As illustrated in Figs. 5A–5C and S1A, the cytotoxicity of the three compounds varied across different tumor cell lines, but all inhibited tumor cell growth and induced cell death. Compound **1** exhibited IC_{50} values of 13.6 ± 1.20, 13.9 ± 1.14, and 19.1 ± 0.34 μmol·L^{-1} for HCT116, HT1080, and HepG2 cells, respectively (Fig. 5A). Compound **2** demonstrated IC_{50} values of 12.0 ± 1.11, 28.3 ± 3.14, and 40.1 ± 4.08 μmol·L^{-1} for HCT116, HT1080, and HepG2 cells, respectively (Fig. 5B). Compound **3** showed IC_{50} values of 3.96 ± 0.31, 4.63 ± 0.56, and 9.42 ± 1.33 μmol·L^{-1} for HCT116, HT1080, and HepG2 cells, respectively (Fig. 5C). Morphologically, tumor cells treated with compounds **1**, **2**, and **3** exhibited varying degrees of cytoplasmic vacuolation (Figs. 5D and S1A−C), a characteristic feature of paraptosis. Paraptosis is a specific form of PCD characterized by extensive cytoplasmic vacuolation, including dilation of the ER and/or mitochondria [20-21]. ER Tracker staining revealed that these vesicles likely originated from the ER (Fig. 5E). Previous research has indicated that progressive protein accumulation triggers paraptosis, and inhibition of protein synthesis by cycloheximide (CHX) can effectively block cytoplasmic vacuolation and paraptosis [21]. Consistently in this study, paraptosis-like cell death was partially rescued by CHX (Fig. 5D). Furthermore, previous studies have shown that disruption of redox balance is another trigger for paraptosis [22]. Consequently, we examined ROS levels following treatment with compounds **1** and **3**. We observed that both compounds significantly increased intracellular ROS levels, comparable to those induced by the positive control H_2O_2 (Fig. 5F). Additionally, NAC, a well-known ROS inhibitor, effectively scavenged ROS in the treated cells.

Intracellular ROS primarily originate from the cytoplasm and various organelles, including the ER and mito-

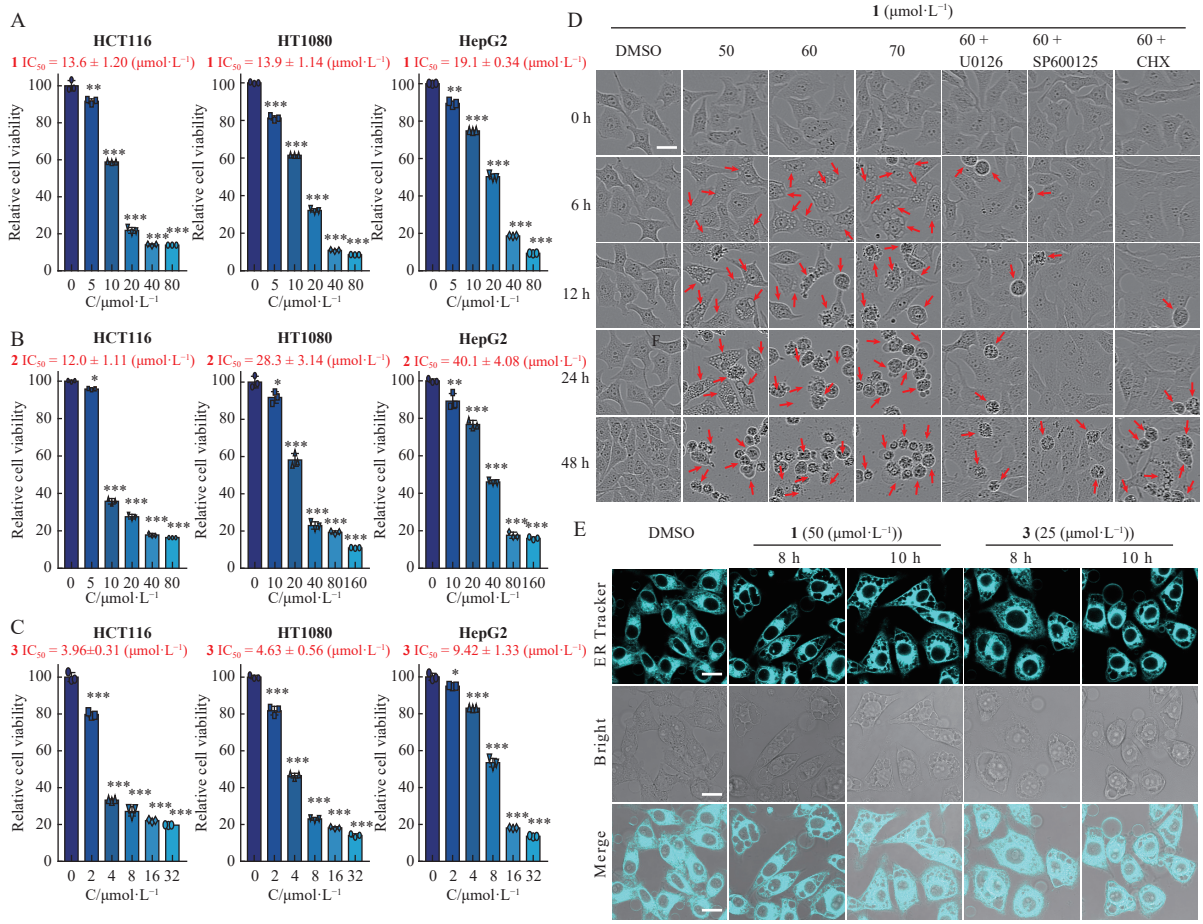

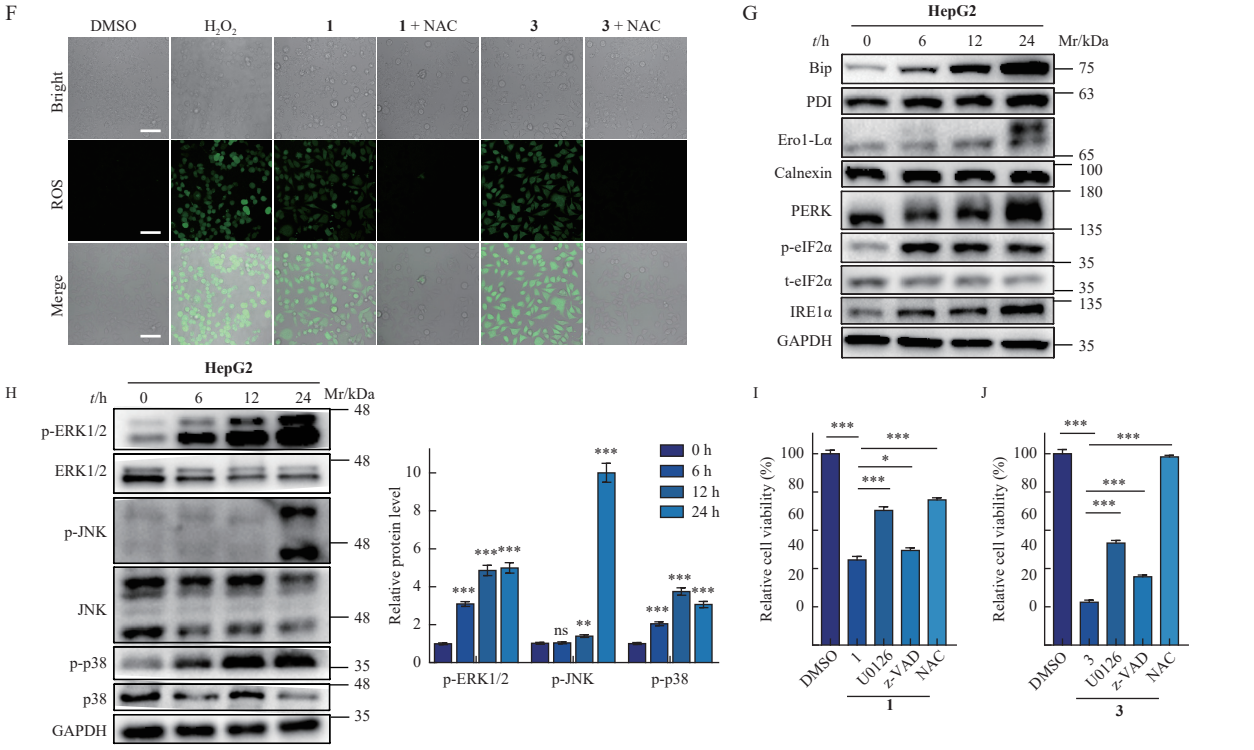

Fig. 5 Compounds 1–3 trigger ER stress-mediated paraptosis-like cell death *via* MAPK signaling. (A–C) The viability of HCT116, HT1080, and HepG2 cells treated with the indicated concentrations of compound 1 (5, 10, 20, 40, and 80 μmol·L^{-1}) (A), compound 2 (5, 10, 20, 40, 80, and 160 μmol·L^{-1}) (B) and compound 3 (2, 4, 8, 16, and 32 μmol·L^{-1}) (C) for 48 h was determined by MTT assay. (D) Morphological changes in HepG2 cells treated with compound 1 at 50, 60, or 70 μmol·L^{-1} alone or with U0126(1 μmol·L^{-1}), SP600125 (2 μmol·L^{-1}), and CHX (5 μmol·L^{-1}) for 6, 12, 24, and 48 h, respectively. (E) ER Tracker was used to indicate the morphological changes in the endoplasmic reticulum in HepG2 cells treated with 1 (50 μmol·L^{-1}) or 3 (25 μmol·L^{-1}) for 8 or 10 h. (F) After treatment of HepG2 cells with compound 1 (60 μmol·L^{-1}) or compound 3 (20 μmol·L^{-1}) for 10 h, intracellular ROS levels were detected by DCFH-DA. (G) Compound 1 induced ER stress. After HepG2 cells were treated with compound 1 (40 μmol·L^{-1}) for the indicated times, the expression of ER stress-related proteins was detected by Western blot assay. (H) Compound 1 hyperactivated the MAPK signaling pathway. HepG2 cells were treated with compound 1 (40 μmol·L^{-1}), and the expression levels of ERK1/2, JNK, and p38 were detected by Western blot assay. (I&J) Viability of HepG2 cells treated with compound 1 (40 μmol·L^{-1}) (I) or compound 3 (20 μmol·L^{-1}) (J) for 10 h alone or in combination with various cell death inhibitors. U0126 (1 μmol·L^{-1}), z-VAD (1 μmol·L^{-1}), and NAC (2 mmol·L^{-1}). $^{*}P < 0.05$, $^{**}P < 0.01$, $^{***}P < 0.001$ *vs* the untreated group. Data are the mean ± SD ($n = 3$).

chondria. Alterations in the ER's redox state can induce ER stress, triggering the unfolding protein response (UPR) [23]. Consequently, we examined whether compounds **1** and **3** affect the expression of ER stress-related proteins. Our findings revealed that after treating HepG2 cells with compounds **1** or **3** for 6, 12, 24, and 48 h, both the PERK-p-eIF2α branch and the IRE1α branch of the UPR were upregulated in a time-dependent manner, and the expression levels of ER stress molecule chaperones PDI, Ero1-Lα, and calnexin increased (Figs. 5G and S1D, F, H). Furthermore, MAPK hyperactivation has been identified as another characteristic of paraptosis [21]. MAPK is involved in various signal transduction processes and can regulate cell proliferation, differentiation, and death. It comprises three family members: ERK1/2, JNK, and p38. Thus, we assessed the impact of compounds **1** and **3** on the MAPK signaling pathway in HepG2 cells. The results demonstrated that compounds **1** and **3** can induce the upregulation of phosphorylated ERK, JNK, and p38, thereby activating the MAPK signaling pathway, which further triggers paraptosis-like cell death in cancer cells (Figs. 5H and S1E, G, I). Subsequently, compounds **1** or **3** were used to treat cells simultaneously with the ERK1/2 inhibitor U0126 and JNK inhibitor SP600125, respectively. The results showed that U0126 and SP600125 significantly reduced the number of cells with cytoplasmic vacuolation and largely reversed the cell death induced by compounds **1** and **3** within 48 h (Figs. 5D and S1B–C). Collectively, these findings suggest that the treatment of tumor cells with compounds **1** and **3** induces excessive ROS accumulation and ER stress, consequently leading to paraptosis-like cell death *via* hyperactivation of the MAPK signaling pathway.

Costunolide and dehydrocostus lactone, the primary sesquiterpene lactones in *A. costus*, have been reported to induce apoptosis and cell cycle arrest [13]. In this study, we investigated whether compounds **1** and **3** could elicit similar effects. As illustrated in Figs. 5I & J, cell death was significantly mitigated by the ROS scavenger NAC and U0126. A modest reduction in cell death was observed in cells treated

with the pan-caspase inhibitor z-VAD. Consistent with these findings, annexin V and PI staining revealed a small fraction of early apoptotic cells (Annexin V + PI-population) induced by compounds **1** and **3**, comprising approximately 26.5% and 32.2% of all dead cells, respectively (Fig. S2A). Assessment of various apoptosis-related proteins, including bcl-2, bax, puma, noxa, and caspase-3, corroborated the conclusion that compounds **1** and **3** could indeed trigger apoptosis (Figs. S2B&C). However, no cell cycle arrest was observed following treatment with compounds **1** and **3** (Figs. S2D–F), potentially due to the destruction of the *α*-methylene-γ-butyrolactone moiety in the sesquiterpene lactones during the dimerization process.

Sesquiterpene dimers are commonly reported, with the majority being homodimers, such as guaiane-type sesquiterpenoid dimers from the Asteraceae family and lindenane-type sesquiterpenoid dimers from the Chloranthaceae family. Biosynthetically, compounds **1**–**3** likely originate from an eudesmane sesquiterpene (diene) and a guaiane sesquiterpene (dienophile) through a Diels−Alder cycloaddition. To date, only six sesquiterpenoid dimers with this specific carbon framework have been documented, most being olefinic isomerization products [16, 17, 24, 25]. Compounds **1**–**3** represent novel Diels−Alder cycloaddition products, with compounds **2** and **3** exhibiting distinct conformations (11*R*,8′*R*), potentially due to variations in coupling during the Diels−Alder cycloaddition process. Furthermore, compounds **1** and **2**, despite having identical planar structures but different configurations, demonstrated comparable cytotoxicity. This similarity in cytotoxic effects may be attributed to the 2-methylacryloyl moiety, which functions as a Michael receptor and constitutes the primary pharmacophore responsible for their cytotoxicity.

Experimental

General experimental procedures

Optical rotations were measured using an Autopol VI polarimeter. Electronic circular dichroism (ECD) spectra were recorded with an Applied Photophysics spectropolarimeter. UV spectra were obtained using a Shimadzu UV2700 spectrophotometer. Infrared (IR) spectra were acquired on a Bruker PMA-50 infrared spectrometer with KBr pellets. Nuclear magnetic resonance (NMR) spectra were collected on a Bruker AM-500 MHz spectrometer. High-resolution electrospray ionization mass spectrometry (HR-ESI-MS) data were measured using an Agilent 1290 UPLC/6540 Q-TOF mass spectrometer. Semi-preparative high-performance liquid chromatography (HPLC) was performed on an Agilent 1260 instrument equipped with a Zorbax SB-C_{18} column (9.4 mm × 250 mm, 5 μm, Agilent). Column chromatography (CC) was conducted using silica gel (200–300 mesh, Qingdao Marine Chemical Inc., China), MCI-gel CHP20P (75–150 μm, Mitsubishi Chemical Co., Japan), and Sephadex LH-20 (GE Healthcare, USA). Thin-layer chromatography (TLC) was carried out on silica gel GF_{254} plates (Qingdao Marine Chemical, Inc. China).

Plant material

The leaves of *A. costus* were collected in September 2020 from Shangri-La City, Yunnan Province, China. The plant material was identified by Prof. JI Yunheng from the Kunming Institute of Botany. A voucher specimen (No. HY202009-1) was deposited at the State Key Laboratory of Phytochemistry and Plant Resources in West China.

Extraction and isolation

The dried and powdered leaves of *A. costus* (15.0 kg) underwent three successive extractions with 95% methanol to yield a crude extract. Subsequently, the methanol extract was suspended in water and subjected to three additional extractions with ethyl acetate (EtOAc). After solvent removal, the EtOAc extract (611.5 g) was fractioned using a silica gel column with petroleum ether–EtOAc (gradient from 1 : 0 to 0 : 1, *V/V*) to yield eight fractions (Fr. A–H). Fr. F (65.3 g) was further separated using an MCI gel column (MeOH/H_2O, 50%→100%, *V/V*) to produce eight fractions (Fr. F.1–8). Fr. F.7 (8.2 g) underwent additional separation using a silica gel column with a gradient of dichloromethane–methanol (1 : 0→20 : 1, *V/V*) to yield eight fractions (Fr. F.7.1–8). Fr. F.7.6 (239.8 mg) was separated by a Sephadex LH-20 column (acetone) and further purified using semi-preparative HPLC (57% MeCN in H_2O, 3.0 mL·min^{-1}) to afford **1** (8.8 mg, t_R = 16.1 min). Fr. F.7.8 (522.1 mg) was separated by a Sephadex LH-20 column (chloroform−methanol 1 : 1) and further purified using semi-preparative HPLC (55% MeCN in H_2O, 3.0 mL·min^{-1}) to afford **2** (9.2 mg, t_R = 16.6 min) and **3** (3.6 mg, t_R = 17.3 min).

Auckcostusolide A (**1**). Colorless needle crystals, $[\alpha]_D^{20}$+156.5 (*c* 0.09, MeOH); UV (MeOH) λ_{max} (logε) 195 (3.62) nm; CD (MeOH) λ_{max} ($\Delta\varepsilon$) 237 (+4.05) 217 (−3.06), 302 (−1.36) nm; IR (KBr) ν_{max} 3433, 2929, 1752, 1713, 1640, 1452, 1295, 1164, 906 cm^{-1}; ^{1}H NMR (500 MHz) and ^{13}C NMR (125 MHz) data see Table 1; HR-ESI-MS *m/z* 585.2827 [M + Na]$^+$ (Calcd. for $C_{34}H_{42}NaO_7^+$, 585.2828).

Auckcostusolide B (**2**). White amorphous powder, $[\alpha]_D^{20}$ +69.0 (*c* 0.10, MeOH); UV (MeOH) λ_{max} (log ε) 195 (3.45) nm; CD (MeOH) λ_{max} ($\Delta\varepsilon$) 304 (3.00), 217 (−7.12) nm; IR (KBr) ν_{max} 3429, 2930, 1768, 1710, 1638, 1450, 1296, 1165, 1057, 903 cm^{-1}; ^{1}H NMR (500 MHz) and ^{13}C NMR (125 MHz) data see Table 1; HR-ESI-MS *m/z* 585.2827 [M + Na]$^+$ (Calcd. for $C_{34}H_{42}NaO_7^+$, 585.2828).

Auckcostusolide C (**3**). White amorphous powder, $[\alpha]_D^{20}$+63.5 (*c* 0.13, MeOH); UV (MeOH) λ_{max} (logε) 195 (3.55) nm; CD (MeOH) λ_{max} ($\Delta\varepsilon$) 305 (2.37) 229 (−4.66) nm; IR (KBr) ν_{max} 3436, 2931, 1766, 1711, 1643, 1450, 1298, 1170, 1108, 907 cm^{-1}; ^{1}H NMR (500 MHz) and ^{13}C NMR (125 MHz) data (Table 1); HR-ESI-MS *m/z* 615.2933 [M + Na]$^+$ (Calcd. for $C_{35}H_{44}NaO_8^+$, 615.2934).

X-ray crystallographic data for auckcostusolide A (1): $2(C_{34}H_{42}O_7)\cdot 3(H_2O)$, M = 1179.39, a = 6.7555(4) Å, b = 34.1300(18) Å, c = 13.3242(7) Å, α = 90°, β = 93.355(2)°, γ = 90°, V = 3066.8(3) Å^3, T = 100.(2) K, space group P 1211, Z = 2, μ (Cu Kα) = 0.740 mm^{-1}, 40669 reflections measured, 10951 independent reflections (R_{int} = 0.0835). The final R_1 values were 0.0896 (I > 2 σ(*I*)). The final *wR* (F^2) values were 0.2340 (I > 2 σ(*I*)). The final R_1 values

were 0.0926 (all data). The final *wR* (F^2) values were 0.2401 (all data). The goodness of fit on F^2 was 1.042. Flack parameter = 0.11(9). Crystallographic data for auckcostusolide A (1) have been deposited in the Cambridge Crystallographic Data Center (deposition number: CCDC 2293000).

Cell culture

Human hepatocellular carcinoma (HepG2), fibrosarcoma (HT1080), and colorectal cancer (HCT116) cell lines were cultivated in DMEM or RPMI 1640 (Gibco) medium supplemented with 10% fetal bovine serum (Gibco), 10 000 $U \cdot mL^{-1}$ penicillin, and 100 $mg \cdot mL^{-1}$ streptomycin. The cells were maintained at 37 °C in a humidified atmosphere containing 5% CO_2 and were utilized during their logarithmic growth phase. HepG2 and HT1080 cell lines were obtained from the China Center for Type Culture Collection (CCTCC), while HCT116 cells were provided by Professor YAN Li from Yunnan University, China.

Cell viability (MTT) assay

HepG2, HT1080, and HCT116 cell lines were utilized for this study. Cells in the logarithmic growth phase were subjected to trypsinization and subsequently seeded into 96-well plates at a density of 6000 cells per well. The cytotoxic activity of the compounds was evaluated using the MTT proliferation assay. Compound stock solutions were prepared in DMSO, and cells were exposed to compound concentrations ranging from 2 to 180 $\mu mol \cdot L^{-1}$ for a duration of 48 hours. The half-maximal inhibitory concentration (IC_{50}) was determined using GraphPad Prism 7 software, based on the concentration-activity relationship. Results are presented as Mean ± SD.

Detection of cell morphology

HepG2 and HT1080 cells were seeded into 12-well plates at a density of 1.5×10^5 cells/well. The cells were subsequently treated with specified concentrations of compounds **1** or **3** and/or inhibitors for 48 h. Long-term dynamic live cell imaging was conducted using an IncuCyte S3 system (Thermo Fisher Scientific, USA).

ROS detection

The ROS content in HepG2 cells was assessed using DCFH-DA (Meilunbio, Dalian, China). HepG2 cells were seeded in confocal dishes at a density of 5×10^4 cells per well. The cells were treated with the compound for 10 h, after which the supernatant was discarded. DCFH-DA was then applied at a final concentration of 10 $\mu mol \cdot L^{-1}$. Subsequently, 500 μL of DCFH-DA diluent was added to each well and incubated at 37 °C for 30 min in dark conditions. ROS levels were then detected using laser scanning confocal microscopy (Leica, TSC SP8 X).

Western blot assay

Total protein was extracted from cells using RIPA (Invitrogen, FNN0011) lysis buffer. Protein concentration was determined using a BCA kit (Biosharp, BL521A). Proteins were separated by 12% sodium dodecyl-sulfate polyacrylamide gel electrophoresis (SDS-PAGE) and transferred to PVDF membranes. The membranes were blocked with phosphate-buffered saline with Tween 20 (PBST) containing 5% skimmed milk for 1 h and incubated with primary antibodies overnight at 4 °C. The primary antibodies used in this study were as follows: GAPDH (1 : 30 000, proteintech, 60004-1-Ig), PDI (1 : 1000, Cell Signaling Technology, 3501), IRE1α (1 : 1000, Cell Signaling Technology, 3294), Calnexin (1 : 1000, Cell Signaling Technology, 2433), Ero1-Lα (1 : 1000, Cell Signaling Technology, 3264), Bip (1 : 1000, Cell Signaling Technology, 3183), PERK (1 : 1000, Cell Signaling Technology, 5683), p-eIF2α (1 : 1000, Cell Signaling Technology, 3398), p-SAPK/JNK (1 : 1000, Cell Signaling Technology, 4668), JNK (1 : 1000, Zen-Bio, R24780), p-p38 (1 : 1000, Cell Signaling Technology, 4511), p38 (1 : 1000, Zen-Bio, R25239), p-ERK1/2 (1 : 1000, Zen-Bio, 301245), ERK1/2 (1 : 1000, Zen-Bio, R22685). Subsequently, the membranes were washed with PBST and incubated with secondary antibodies for 2 h. The bands were visualized using ChemiDoc™ XRS + (Bio-Rad, USA) and quantitatively analyzed using Image Lab 5.2.

Endoplasmic reticulum tracking

HepG2 cells were seeded in confocal dishes at a density of 5×10^4 cells per well. After 12 h, the culture medium was replaced with 2 mL of fresh medium containing either 50 $\mu mol \cdot L^{-1}$ of compound **1** or 25 $\mu mol \cdot L^{-1}$ of compound **3**. Following 8 or 10 h of incubation, the medium was discarded and the cells were rinsed three times with PBS buffer. Subsequently, cells were fixed with 4% formaldehyde at 37 °C for 15 min and washed three times with PBS. The cells were then incubated with 1.2 mL PBS containing ER-Tracker Blue-White DPX (200 $nmol \cdot L^{-1}$, Yeasen 40761ES50) for 30 min. Fluorescence was monitored using laser scanning confocal microscopy (Leica, TSC SP8 X).

Apoptosis assessment

The Annexin V-FITC/PI apoptosis detection kit (4A Biotech Co., Ltd., FXP018) was utilized for apoptosis analysis. HepG2 cells (5×10^5) were seeded in 60-mm dishes and exposed to various concentrations of compound **1** or compound **3** for 36 h. The cells were then trypsinized and centrifuged (1200 $r \cdot min^{-1}$, 5 min, 4 °C). Subsequently, the cells were washed thrice with cold PBS. The cell pellet was resuspended in 300 μL of 1 × Binding buffer. Following this, 5 μL of Annexin V-FITC and 10 μL of PI staining solutions were added to each well and gently mixed. After incubating the cells in darkness at 37 °C for 15 min, 200 μL of PBS was added and mixed gently. Finally, the percentage of cell apoptosis was quantified using flow cytometry (BD FACSCelesta™).

Cell cycle analysis

The cell cycle analysis was conducted as previously described [26]. For cell cycle distribution analysis, HepG2 cells (5×10^5) were seeded in 60-mm dishes and treated with varying concentrations of Compound **1** or Compound **3** for 36 h. DMSO-treated cells served as controls. The cells were harvested and fixed in 70% ethanol. After washing with PBS, the cells were resuspended with RNase A (200 $\mu g \cdot mL^{-1}$) (BioFROXX, 1341MG025) solution and incubated in a 37 °C water bath for 10 min. The supernatant was removed, and PI dye (BIOFROXX, A8260, 100 $\mu g \cdot mL^{-1}$) was added. The cells were then incubated in darkness at 37 °C for 15 min, followed by detection using flow cytometry (BD FACSCelesta™).

Statistical analysis

Data from three independent experiments were analyzed using Prism 7.0 (GraphPad Software). Results are presented as Mean ± SD. Differences between two groups were assessed using Student's *t*-test. A *P*-value less than 0.05 was considered statistically significant.

Conclusions

In summary, three novel sesquiterpenoid heterodimers were isolated from the leaves of *A. costus*. These compounds were formed through a Diels−Alder cycloaddition, involving an eudesmane sesquiterpene as a diene and a guaiane sesquiterpene as a dienophile. Compounds **1** and **2** exhibited opposite configurations at C-11 and C-8′ due to variations in the relative positions of the two sesquiterpenoids during the Diels−Alder cycloaddition process. Furthermore, the cytotoxic effects of compounds **1**–**3** against multiple tumor cells were evaluated, and their potential mechanisms were investigated. Compounds **1** and **3** induced ROS accumulation and ER stress (PERK-p-eIF2α branch and IRE1α branch)-mediated cytoplasmic vacuolation, characteristic of paraptosis-like cell death. Additionally, compounds **1** and **3** hyperactivated the MAPK signaling pathway. Pharmacological inhibition of the ERK and JNK pathway significantly reduced cytoplasmic vacuolation and mitigated cell death triggered by compounds **1** and **3**. These findings underscore the potential of sesquiterpenoid heterodimers from *A. costus* in cancer treatment.

References

[1] Sperandio S, De Belle I, Bredesen DE. An alternative, nonapoptotic form of programmed cell death [J]. *Proc Natl Acad Sci U S A*, 2000, **97**(26): 14376-14381.

[2] Hanson S, Dharan A, Jinsha PV, *et al*. Paraptosis: a unique cell death mode for targeting cancer [J]. *Front Pharmacol*, 2023, **14**: 1-28.

[3] Fontana F, Raimondi M, Marzagalli M, *et al*. The emerging role of paraptosis in tumor cell biology: perspectives for cancer prevention and therapy with natural compounds [J]. *Biochim Biophys Acta-Reviews Cancer*, 2020, **1873**(2): 188338.

[4] Lee D, Kim IY, Saha S, *et al*. Paraptosis in the anti-cancer arsenal of natural products [J]. *Pharmacol Ther*, 2016, **162**: 120-133.

[5] Wan JY, Yao H, Zhang CF, *et al*. Red American ginseng enhances the effect of fluorouracil on human colon cancer cells *via* both paraptosis and apoptosis pathways [J]. *J Appl Biomed*, 2018, **16**(4): 311-319.

[6] Zhuang KY, Xia Q, Zhang SS, *et al*. A comprehensive chemical and pharmacological review of three confusable Chinese herbal medicine — *Aucklandiae radix, Vladimiriae radix*, and *Inulae radix* [J]. *Phytother Res*, 2021, **35**(12): 6655-6689.

[7] Pandey MM, Rastogi S, Rawat AKS. *Saussurea costus*: botanical, chemical and pharmacological review of an ayurvedic medicinal plant [J]. *J Ethnopharmacol*, 2007, **110**(3): 379-390.

[8] Wang C, Chen Y, Zhao Y, *et al*. Radix aucklandiae seed edible oil and preparation method thereof [P]. CN114874841A. 2022.

[9] Koelz WN. Notes on the ethnobotany of lahul, a province of the punjab [J]. *Pharm Biol*, 1979, **17**(1): 1-56.

[10] Kuniyal CP, Rawat YS, Oinam SS, *et al*. Kuth (*Saussurea lappa*) cultivation in the cold desert environment of the Lahaul valley, northwestern Himalaya, India: arising threats and need to revive socio-economic values [J]. *Biodivers Conserv*, 2005, **14**(5): 1035-1045.

[11] Ali SI, Venkatesalu V. Botany, traditional uses, phytochemistry and pharmacological properties of *Saussurea costus*–an endangered plant from Himalaya-A review [J]. *Phytochem Lett*, 2022, **47**: 140-155.

[12] Huang ZC, Wei CL, Yang K, *et al*. Aucklandiae Radix and Vladimiriae Radix: a systematic review in ethnopharmacology, phytochemistry and pharmacology [J]. *J Ethnopharmacol*, 2021, **280**: 114372.

[13] Li QJ, Wang ZG, Xie Y, *et al*. Antitumor activity and mechanism of costunolide and dehydrocostus lactone: two natural sesquiterpene lactones from the Asteraceae family [J]. *Biomed Pharmacother*, 2020, **125**: 109955.

[14] Sun CM, Syu WJ, Don MJ, *et al*. Cytotoxic sesquiterpene lactones from the root of *Saussurea lappa* [J]. *J Nat Prod*, 2003, **66**(9): 1175-1180.

[15] Lai ST, Zhang T, Wang HQ, *et al*. Two new sesquiterpene dimers isolated from the roots of *Saussurea lappa* (Yunmuxiang). [J]. *J Asian Nat Prod Res*, 2022, **24**: 490-495.

[16] Lyu HY, Bao MY, Io CC, *et al*. Sesquiterpenoids from the roots of *Aucklandia costus* and their anti-inflammatory activities [J]. *Fitoterapia*, 2023, **169**: 105604.

[17] Han JS, Kim JG, Linh Le TP, *et al*. Targeted isolation of sesquiterpene lactone dimers from *Aucklandia lappa* guided by LC-HRMS/MS-based molecular networking [J]. *Phytochemistry*, 2023, **206**: 113557.

[18] Shati AA, Alkahtani MA, Alfaifi MY, *et al*. Secondary metabolites of *Saussurea costus* leaf extract induce apoptosis in breast, liver, and colon cancer cells by caspase-3-dependent intrinsic pathway [J]. *Biomed Res Int*, 2020, **2020**: 1608942.

[19] Ha TJ, Jang DS, Lee JR, *et al*. Cytotoxic effects of sesquiterpene lactones from the flowers of *Hemisteptia lyrata* B [J]. *Arch Pharm Res*, 2003, **26**(11): 925-928.

[20] Sperandio S, Poksay K, Belle I, *et al*. Paraptosis: mediation by MAP kinases and inhibition by AIP-1/Alix [J]. *Cell Death Differ*, 2004, **11**(10): 1066-1075.

[21] Li GN, Zhao XJ, Wang Z, *et al*. Elaiophylin triggers paraptosis and preferentially kills ovarian cancer drug-resistant cells by inducing MAPK hyperactivation [J]. *Signal Transduct Target Ther*, 2022, **7**(1): 317.

[22] Nguyen PL, Lee CH, Lee H, *et al*. Induction of paraptotic cell death in breast cancer cells by a novel pyrazolo[3, 4 - h]quinoline derivative through ROS production and endoplasmic reticulum stress [J]. *Antioxidants*, 2022, **11**(1): 117.

[23] Zhang Z, Zhang L, Zhou L, *et al*. Redox signaling and unfolded protein response coordinate cell fate decisions under ER stress [J]. *Redox Biol*, 2019, **25**: 101047.

[24] Wu ZL, Wang Q, Dong HY, *et al*. Five rare dimeric sesquiterpenes exhibiting potential neuroprotection activity from *Vladimiria souliei* [J]. *Fitoterapia*, 2018, **128**: 192-197.

[25] Wu ZL, Li JY, Sun ZS, *et al*. Vlasouliodes A-D, four new C30 dimeric sesquiterpenes exhibiting potential inhibition of MCF-7 cells from *Vladimiria souliei* [J]. *Fitoterapia*, 2022, **161**: 105234.

[26] Wei RR, Zhao YQ, Wang J, *et al*. Tagitinin C induces ferroptosis through PERK-Nrf2-HO-1 signaling pathway in colorectal cancer cells. [J]. *Int J Biol Sci*, 2021, **17**(11): 2703-2717.

Cite this article as: XIAO Longgao, ZHAO Yueqin, DING Xiao, *et al*. Eudesmane-guaiane sesquiterpenoid dimers from *Aucklandia costus* trigger paraptosis-like cell death *via* ROS accumulation and MAPK hyperactivation [J]. *Chin J Nat Med*, 2024, **22**(11): 1011-1019.